

Quasar Clustering in Cosmological Hydrodynamic Simulations: Evidence for mergers

Colin Degraf¹, Tiziana Di Matteo¹, Volker Springel²

¹ *McWilliams Center for Cosmology, Carnegie Mellon University, 5000 Forbes Avenue, Pittsburgh, PA 15213, USA*

² *Max-Planck-Institut für Astrophysik, Karl-Schwarzschild-Straße 1, 85740 Garching bei München, Germany*

Accepted 200? ???? ??. Received 2008 ???? ??; in original form 2008 xx

ABSTRACT

We examine the clustering properties of a population of quasars drawn from fully hydrodynamic cosmological simulations that directly follow black hole growth. We find that the black hole correlation function is best described by two distinct components: contributions from BH pairs occupying the same dark matter halo ('1-halo term', $\xi_{\text{BH,1h}}$) which dominate at scales below $\sim 300 \text{ kpc h}^{-1}$, and contributions from BHs occupying separate halos ('2-halo term', $\xi_{\text{BH,2h}}$) which dominate at larger scales. From the 2-halo BH term we find a typical host halo mass for faint-end quasars (those probed in our simulation volumes) ranging from $M \sim 10^{11}$ to a few $10^{12} M_{\odot}$ from $z = 5$ to $z = 1$ respectively (consistent with the mean halo host mass). The BH correlation function shows a luminosity dependence as a function of redshift, though weak enough to be consistent with observational constraints. At small scales, the high resolution of our simulations allows us to probe the 1-halo clustering in detail, finding that $\xi_{\text{BH,1h}}$ follows an approximate power law, lacking the characteristic decrease in slope at small scales found in 1-halo terms for galaxies and dark matter. We show that this difference is a direct result of a boost in the small-scale quasar bias caused by galaxies hosting multiple quasars (1-subhalo term) following a merger event, typically between a large central subgroup and a smaller, satellite subgroup hosting a relatively small black hole. We show that our predicted small-scale excess caused by such mergers is in good agreement with both the slope and amplitude indicated by recent small-scale measurements. Finally, we note the excess to be a strong function of halo mass, such that the observed excess is well matched by the multiple black holes of intermediate mass ($10^7 - 10^8 M_{\odot}$) found in hosts of $M \sim 4 - 8 \times 10^{11} M_{\odot}$, a range well probed by our simulations.

1 INTRODUCTION

With supermassive black holes being found at the centre of most galaxies (Kormendy & Richstone 1995), interest in quasars has increased significantly, with substantial investigation into fundamental relations between black hole masses and their host galaxies' properties (Magorrian et al. 1998; Ferrarese & Merritt 2000; Gebhardt et al. 2000; Tremaine et al. 2002; Graham & Driver 2007). In addition to these relations, statistical studies of the spatial clustering of quasars provide the potential to better understand the relation between quasars, their hosts and the underlying dark matter distribution, as well as estimate quasar lifetimes (see, e.g., Haiman & Hui 2001; Martini & Weinberg 2001) across a relatively large range of redshift. For example, strong clustering would suggest quasars should reside in massive groups. If so, they should be rare and in order to reproduce the quasar luminosity density, they must have long lifetimes. Conversely, low correlation would suggest more common quasars, and thus shorter quasar lifetimes.

Early studies of quasar clustering produced varying re-

sults for the clustering amplitude, with no clear agreement on overall evolution with redshift, some suggesting minimal or decreasing clustering evolution (Mo & Fang 1993; Croom & Shanks 1996), while others found an increase in clustering with redshift (Kundic 1997; La Franca et al. 1998). These findings were generally poorly constrained due to the small sizes of available quasar samples. With the emergence of large scale surveys such as Sloan Digital Sky Survey (York et al. 2000) and the Two-degree Field QSO Redshift Survey (Lewis et al. 2002), substantially larger catalogs have been compiled, permitting more detailed investigation into the clustering properties of quasars, and many recent studies have been made into this area (e.g. La Franca et al. 1998; Porciani et al. 2004; Croom et al. 2005; Shen et al. 2007; Myers et al. 2007a; da Ângela et al. 2008; Shen et al. 2009b; Ross et al. 2009). These recent studies have found evidence for an increase in clustering amplitude with redshift (La Franca et al. 1998; Porciani et al. 2004), primarily for $z > 2$, in agreement with predictions from simulations (see, e.g. Bonoli et al. 2009; Croton 2009).

In addition to overall evolution, the luminosity depen-

dence (if any) of large-scale clustering can provide significant insight into what quasar populations dominate different luminosity ranges. For example, the model of Hopkins et al. (2005a,b,c,d, 2006) suggests that bright and faint quasars are similar objects which are observed at different phases of their lifetimes, rather than being fundamentally different populations of quasars (as simpler, 'on-off' models assume). This model would suggest that both bright and faint quasars should populate similar halos. Thus, while there may be some correlation between peak luminosity and host halo mass, clustering dependence on instantaneous luminosity should be relatively weak, particularly when compared to more traditional 'on-off' models of quasar luminosity (Lidz et al. 2006). Recent observational studies have generally found a lack of luminosity dependence in the correlation function (see, e.g., Croom et al. 2005; Myers et al. 2007a; da Ângela et al. 2008), though Shen et al. (2009b) found evidence for some, though weak, luminosity dependence. Several semi-analytic models have also been used, finding differing luminosity dependences, such as a significant dependence for sufficient luminosity ranges, but limited when considering only luminosities probed by observation (Bonoli et al. 2009), or weak dependence at low redshift ($z < 1$), but stronger at higher redshift (Croton 2009).

In addition to large scale behavior, the possibility of excess quasar clustering on very small scales has arisen in several recent studies. While some observed quasar pairs are believed to be the result of gravitationally lensed quasars, it has been proposed that others may be physically distinct quasar binaries, which would suggest quasars cluster much more strongly on small scales than extrapolation of large scale clustering would imply (Djorgovski 1991; Hewett et al. 1998; Kochanek et al. 1999; Mortlock et al. 1999), suggesting a connection between galaxy mergers and quasar activity (see, e.g. Kochanek et al. 1999). However, investigating the smallest scale clustering has typically been problematic due to observational limitations (such as fiber collisions preventing small-separation pairs from being distinguished as distinct objects) and sample sizes insufficient for probing the smallest scales, where quasar pairs are rare. There have been several studies probing clustering at sub-Mpc scales, generally finding no excess clustering relative to an extrapolation of the large-scale clustering behavior (see, e.g. Shen et al. 2009a; Padmanabhan et al. 2009). However, these studies have been limited to scales above 100 kpc h^{-1} , while several recent studies have managed to probe even smaller scales, where they do indeed find a significant excess (Hennawi et al. 2006; Myers et al. 2007b, 2008).

In particular, Hennawi et al. (2006) studied binary quasars from SDSS and 2dF Quasar Survey to compute quasar clustering for scales as small as 20 kpc h^{-1} (comoving), and found significant excess clustering relative to the large scale extrapolation (by an order of magnitude at comoving scales below 100 kpc h^{-1} , and growing stronger with decreasing scale). This excess implies that the quasars are more strongly clustered than galaxies at these small scales, supporting the theory that quasar activity is triggered by galaxy interactions. Using the quasar sample from Myers et al. (2007a), Myers et al. (2007b) found only a slight excess in small-scale clustering, and put an upper limit for the excess at a factor of 4.3 ± 1.3 for physical scales of $\sim 28 \text{ kpc h}^{-1}$. They suggest that the significantly larger

excess of Hennawi et al. (2006) is a result of a selection effect, possibly due to studies tending to target tracers of the Ly α forest, causing a bias toward $z > 2$, which may be more highly clustered. Myers et al. (2008) used a complete spectroscopic sample of quasars over physical scales of $23.7\text{--}29.9 \text{ kpc h}^{-1}$ from SDSS to find an excess clustering factor of ~ 4 , consistent with the upper limit of Myers et al. (2007b), which, while 2σ below the excess found by Hennawi et al. (2006), nonetheless supports the general finding of a clustering excess which may be a result of galaxy interactions.

In this paper, we use cosmological hydrodynamic simulations which directly model the growth, accretion, and feedback processes of black holes to investigate the properties and underlying causes of black hole clustering. Although the simulation volume limits our analysis to black hole luminosities and host group masses below those typically studied, the self-consistent modeling of black holes allows us to study the clustering behavior without post-processing models. Additionally, the high resolution allows us to investigate clustering behavior at extremely small scales, well below those studied with semi-analytic models, thereby providing a means of using simulations to investigate the observed small-scale excess for the first time, and provide a physical explanation for the underlying cause.

In Section 2 we describe the numerical modeling for the black holes formation and accretion (Section 2.1) the simulation parameters used (Section 2.2), the details of the subgroup finder (Section 2.3) and our method of calculating correlation functions (Section 2.4). In Section 3 we investigate the quasar clustering properties at both large and small scales, and we summarize our results in Section 4.

2 METHOD

2.1 Numerical simulation

In this study, we analyse the set of simulations published in Di Matteo et al. (2008). Here we present a brief summary of the simulation code and the method used. We refer the reader to Di Matteo et al. (2008) for all details.

The code we use is the massively parallel cosmological TreePM-SPH code Gadget2 (Springel 2005), with the addition of a multi-phase modeling of the ISM, which allows treatment of star formation (Springel & Hernquist 2003), and black hole accretion and associated feedback processes (Springel et al. 2005; Di Matteo et al. 2005).

Black holes are simulated with collisionless particles that are created in newly emerging and resolved groups/galaxies. To find these groups, a friends-of-friends group finder is called at regular intervals on the fly (the time intervals are equally spaced in $\log a$, with $\Delta \log a = \log 1.25$), finding groups based on particle separations below a specified cutoff. Each of these groups that does not already contain a black hole is provided with one by turning its densest particle into a sink particle with a seed black hole of fixed mass, $M = 5 \times 10^5 h^{-1} M_{\odot}$. After insertion, the black hole particle grows in mass via accretion of surrounding gas according to $\dot{M}_{\text{BH}} = \frac{4\pi G^2 M_{\text{BH}}^2 \rho}{(c_s^2 + v^2)^{3/2}}$ (Hoyle & Lyttleton 1939; Bondi & Hoyle 1944; Bondi 1952), and by merging with other black holes. Note that within the simulations, it is assumed that accretion is limited to a maximum of 3 times

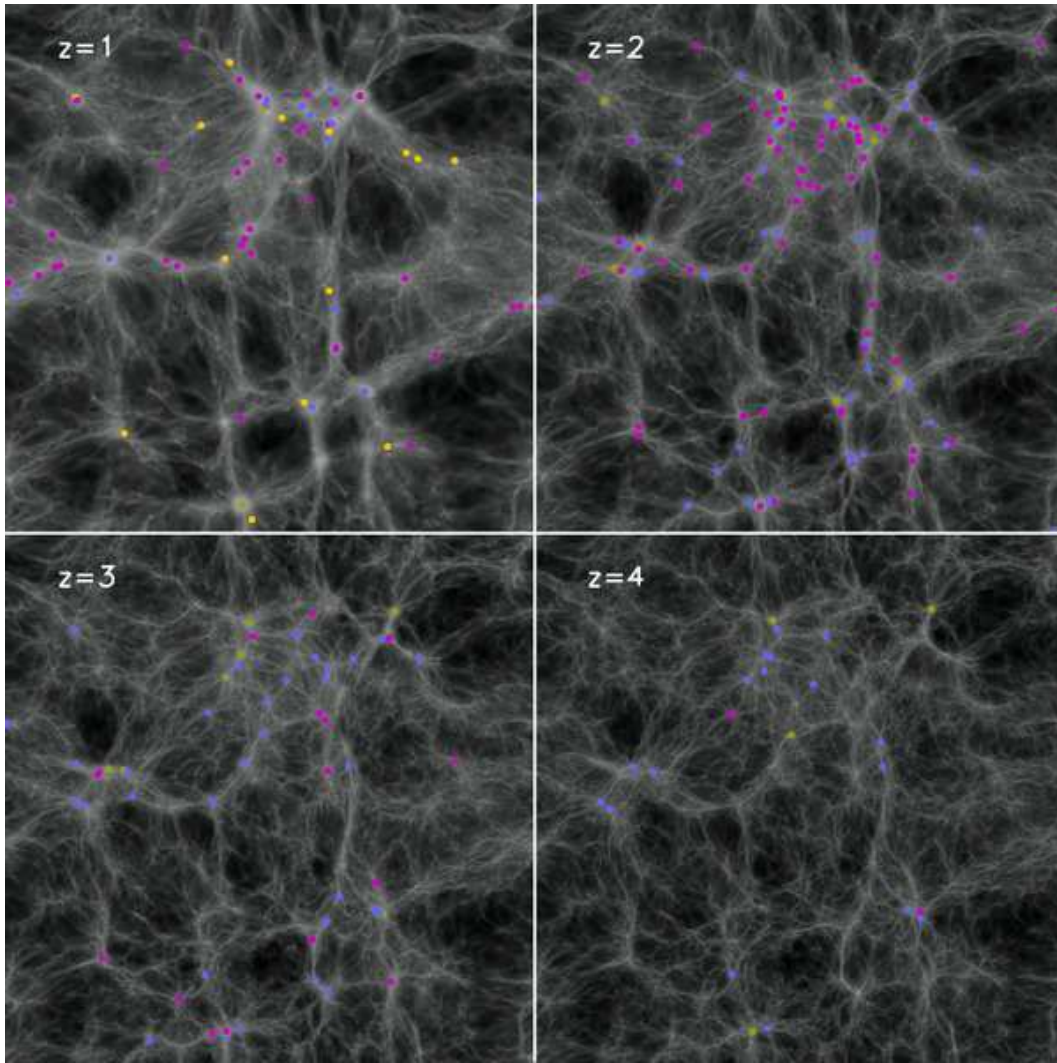


Figure 1. An example of the distribution of black holes in the simulations: The same slice ($2 \text{ Mpc } h^{-1}$ thick) through the D6 simulation at $z=1,2,3,4$. The positions of black holes in different luminosities bins ($L < 10^8 L_\odot$ - Orange; $10^8 L_\odot < L < 10^9 L_\odot$ - Pink; $10^9 L_\odot < L < 10^{10} L_\odot$ - Blue; $L > 10^{10} L_\odot$ - Green.) are plotted on top of the gas density distribution (shown in the gray scale).

the Eddington rate, although very few sources accrete above \dot{M}_{Edd} .

The accretion rate of each black hole is used to compute the bolometric luminosity, $L = \eta \dot{M}_{BH} c^2$ (Shakura & Sunyaev 1973). Here η is the radiative efficiency, and it is fixed at 0.1 throughout the simulation and this analysis. Some coupling between the liberated luminosity and the surrounding gas is expected: in the simulation 5 per cent of the luminosity is (isotropically) deposited as thermal energy in the local black hole kernel, acting as a form of feedback energy (Di Matteo et al. 2005).

2.2 Simulation parameters

Two simulation runs are analysed in this paper to allow for different volume size and resolution. The main parameters are listed in Table 1. Both runs were of moderate volume, with boxsizes of side length $33.75 h^{-1} \text{ Mpc}$ (D6 simulation), and $50 h^{-1} \text{ Mpc}$ (E6). For both simulations $N_p = 2 \times 486^3$ particles were used. The moderate boxsizes prevent the sim-

Table 1. Numerical Parameters

Run	Boxsize $h^{-1} \text{ Mpc}$	N_p	m_{DM} $h^{-1} M_\odot$	m_{gas} $h^{-1} M_\odot$	ϵ $h^{-1} \text{ kpc}$
D6	33.75	2×486^3	2.75×10^7	4.24×10^6	2.73
E6	50	2×486^3	7.85×10^7	1.21×10^7	4.12

N_p : Total number of particles

m_{DM} : Mass of dark matter particles

m_{gas} : Initial mass of gas particles

ϵ : Comoving gravitational softening length

ulations from being run below $z \sim 1$ to keep the fundamental mode linear, but provide a large enough scale to produce statistically significant quasar populations. The limitation on the boxsizes is necessary to allow for appropriate resolution to carry out the subgrid physics in a converged regime (for further details on the simulation methods, parameters and convergence studies see Di Matteo et al. (2008)).

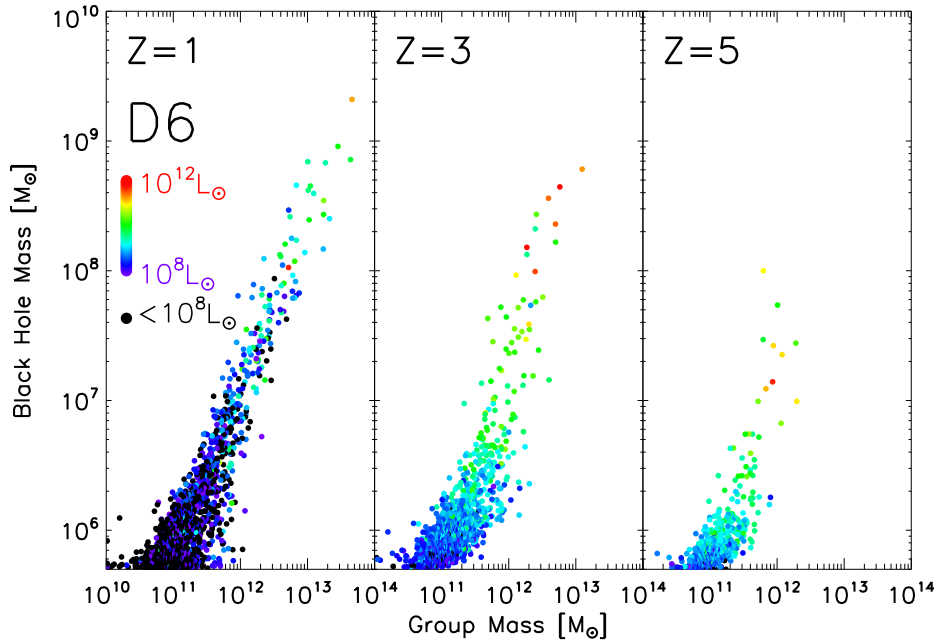


Figure 2. Relation between masses of dark matter halos and their most massive black holes. Color represents bolometric luminosity of the massive BH.

2.3 Subgroup finder algorithm

In addition to the on-the-fly friends-of-friends algorithm used to identify groups, a modified version of the SUBFIND algorithm (Springel et al. 2001) was run on the FoF-identified groups to determine the component subgroups (*i.e.* galaxies) within each group. These subgroups are defined as locally overdense, self-bound particle groups. To identify these regions, the algorithm sorts the particles within the parent group by density, and then analyzes each particle in order of decreasing density. For each particle i , the density of the 32 nearest neighbors are checked. If none are denser than particle i , it forms the basis for a new subgroup. If a single particle denser than i is found, or if the closest two denser particles belong to the same subgroup, particle i is assumed to be a member of that subgroup. If the two nearest particles denser than i are members of different subgroups, these two subgroups are stored as subgroup candidates, and are then joined into a new subgroup also containing i . After checking each particle in this manner, particles are checked for binding within their parent subgroup based on their position relative to the position of the most bound particle, and the velocity relative to the mean velocity of particles in the group. Any particle with positive total energy is considered unbound, and is removed from the subgroup, leaving the group divided up into its component subgroups (galaxies).

2.4 Correlation Function

To investigate the clustering properties of quasars, we use the two-point correlation function $\xi(r)$:

$$dP = \rho_0^2 [1 + \xi(r)] dV_1 dV_2 \quad (1)$$

(Peacock 1999), where dP is the probability of finding one object in each volume element dV_1 and dV_2 , separated by a

distance r , with an average number density of ρ_0 . We use the natural estimator $\xi(r) = \frac{DD}{RR} - 1$ for computing ξ , where DD and RR are the number of pairs of objects found with separation r in the simulation (DD) and in a random distribution of equal spatial density (RR). For calculating RR , we used a random distribution of $N_R = 6 \times 10^5$ objects to find the number of pairs in a random sample, which is then normalized with a factor of $\left(\frac{N_D}{N_R}\right)^2$ (where N_D is the number of objects considered for the DD term) to correct for the increased spatial density of the random sources relative to the BHs in the DD term. Note that the estimator $\xi(r) = \frac{DD - 2DR + RR}{RR}$ (Landy & Szalay 1993) has been shown to be more accurate (as it more effectively accounts for edge effects), but when considering small scales, both estimators provide equivalent results (Kerscher et al. 2000). Indeed, to confirm the validity of the natural estimator, we compared results between the natural estimator and the Landy and Szalay estimator, and found that for the largest scales ($> 5 h^{-1}$ Mpc) at low redshift, they differ by less than 5%, and the discrepancy is well below 1% everywhere else.

3 RESULTS

To illustrate the distribution of quasars (as a function of their luminosity) with respect to the underlying matter distribution, in Figure 1 we plot a slice through the D6 simulation at $z = 1, 2, 3, 4$, with black hole positions indicated by colored dots for four luminosity range bins: $L < 10^8 L_\odot$ - Orange; $10^8 L_\odot < L < 10^9 L_\odot$ - Pink; $10^9 L_\odot < L < 10^{10} L_\odot$ - Blue; $L > 10^{10} L_\odot$ - Green. As expected, as supermassive black holes are hosted by galaxies, the quasars (particularly the most luminous sources) are located in some of the densest regions, with low redshift tending to exhibit more BHs, though at generally fainter luminosities. To characterize the

relation between black hole and host halo mass more precisely, in Figure 2 we show the relation between the group halo mass and the mass of its most massive (central) black hole, with color representing the respective (instantaneous) quasar luminosity. There is a correlation between halo mass and BH mass, and to a lesser extent between halo mass and BH luminosity, with large halos tending to host more massive, more luminous black holes than smaller halos, albeit with significant scatter. This is due to the lightcurve that a black hole has in our simulations (regulated by the complex hydrodynamics, see e.g. Di Matteo et al. 2008; Degraf et al. 2010). We also find that as redshift decreases, the simulation is more densely populated with BHs, which tend to be more massive and less luminous than at earlier redshift.

To study the relation between black holes and other structures, in Figure 3 we show the correlation functions of black holes found in the D6 (solid black) and the E6 (solid pink) simulations for scales between 10 kpc h^{-1} and $\sim 10 \text{ Mpc h}^{-1}$ at $z=1, 3, 5$, with Poisson error bars. Note, the results from the two simulations are very similar, with the higher resolution D6 simulation showing a small boost at small scales (below $\sim 200 \text{ kpc h}^{-1}$). In general, we see ξ_{BH} typically takes the form of a power law (with some possible excess at small scales at $z=1$).

We also divide $\xi_{BH,D6}$ into two terms: a 1-halo term (dashed blue) produced by BH pairs occupying the same host group, and the 2-halo term (dashed green) produced by pairs occupying different groups. As expected, the 2-halo term dominates at large scales (above $\sim 300 \text{ kpc h}^{-1}$), while at smaller scales the 1-halo term dominates, indicating that our small scale clustering is really measuring BH properties within the scales of the host halos. A distinction between the 1-halo and 2-halo terms is expected (as BHs are hosted by galaxies within halos) and is consistent with the theoretical expectations (see, e.g. Cooray & Sheth 2002), as well as what has been found in galaxy correlation functions (see, e.g. Magliocchetti & Porciani 2003; Zehavi et al. 2004).

3.1 Large Scale Clustering

It may be expected that black holes will cluster similarly to their host galaxies (within their halos). To investigate the relation between BH clustering and that of their host halos, in the left column of Figure 4 we plot the 1-halo (blue) and 2-halo (red) contributions to the correlation function (at $z=1, 3$, and 5) for BHs (solid lines) and galaxies (as identified by the subgroup finder described in Section 2.3) populating halos (*i.e.* groups) in the specified mass ranges (dashed lines). These mass ranges were chosen to reproduce the closest agreement between ξ_{BH} and $\xi_{subgroup}$ in the 2-halo regime at each redshift, so as to be used as an indicator of the typical halo mass for BH hosts (at each redshift). The same is shown in the right column of Figure 4 where we only include some of the most luminous BHs in the simulations ($10^9 L_\odot < L_{BH} < 10^{10} L_\odot$, a range which is probed by observations).

For the full BH population, the typical host mass increases slightly with decreasing redshift, from $\sim 10^{11} M_\odot$ to somewhat below $10^{12} M_\odot$ from $z=5$ to $z=1$ respectively. When limited to the luminosity range $10^9 L_\odot < L < 10^{10} L_\odot$, we again find increasing host mass with decreasing redshift, but with a sharper increase up to masses a few times $10^{12} M_\odot$

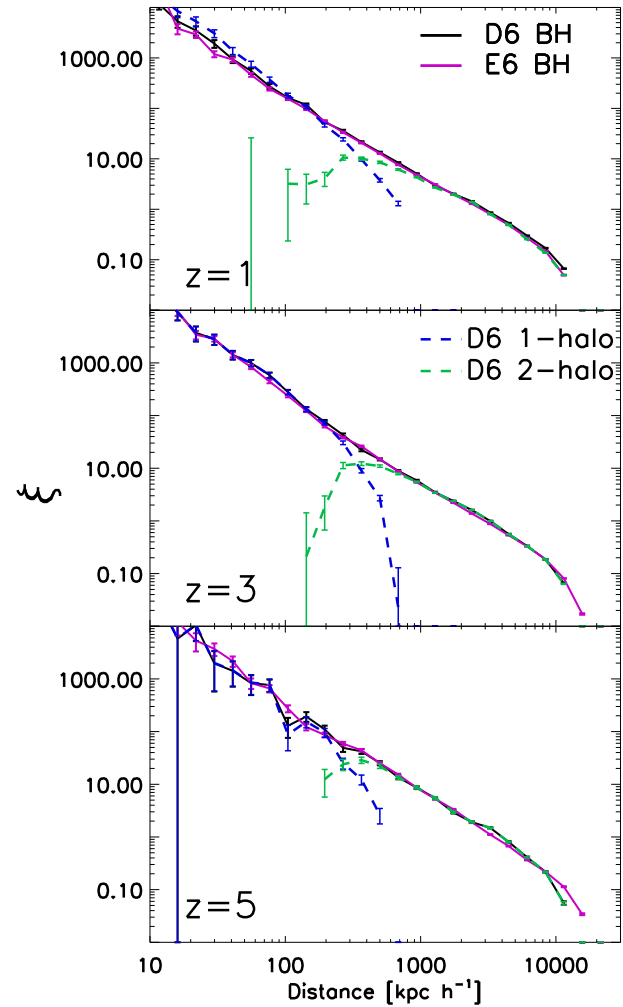


Figure 3. Two point correlation functions for the black holes in the D6 (solid black) and E6 (solid pink) simulations at $z=1, 3, 5$, with the 1-halo and 2-halo terms for the D6 simulation explicitly shown (dashed blue and green, respectively).

at $z=1$ (still in the faint end of the luminosity function, see Degraf et al. 2010).

We compare the typical host mass found in this way to the mean (median) mass of the host halos (see Table 2) for several luminosity ranges, and find that the 2-halo clustering as described above does indeed provide an estimator for the mean host halo mass at the corresponding redshift in the simulations. In addition, the table shows that for a given halo mass the luminosity of its typical BH decreases with time, particularly at low redshift (below $z \sim 2-3$), as seen more generally in Figure 2. This is shown explicitly in the bottom of Table 2, where we calculate the mean and median BH luminosities found within groups of specified halo mass ranges. Note that the mean quasar luminosity actually peaks at $z=3$ for massive ($M > 10^{12} M_\odot$) groups as a result of a few highly luminous sources.

To better characterize the overall clustering strength, and in particular its luminosity dependence and evolution with redshift, we use the correlation length r_0 , defined as the scale at which $\xi(r_0) = 1$ [which we calculate using a linear extrapolation of ξ]. In Figure 5 we plot r_0 versus z for

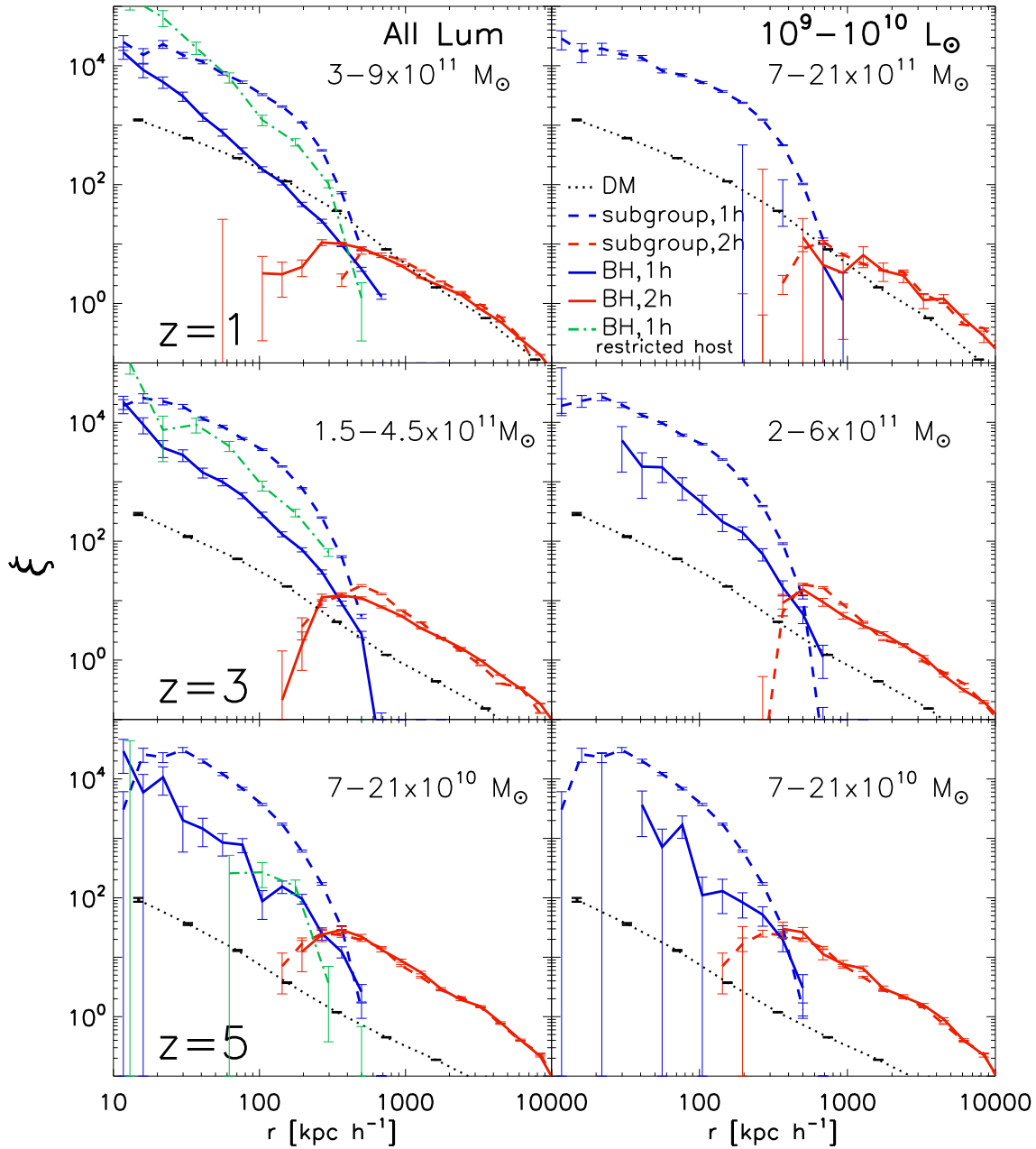


Figure 4. Correlation functions for the D6 simulation BHs (solid) and subgroups within a specified mass range (dashed), at $z=1, 3, 5$, with 1-halo and 2-halo terms plotted separately (blue and red, respectively). The BH correlation function is plotted using all BHs (left) and using only those with $10^9 L_\odot < L_{\text{BH}} < 10^{10} L_\odot$ (right). The mass range for ξ_{group} is chosen so as to find the closest agreement between $\xi_{\text{BH},2\text{h}}$ and ξ_{group} . We also plot $\xi_{\text{BH},1\text{h}}$ using only BHs found in host groups in this fitted mass range (dot-dashed green line).

BHs in several luminosity bins (solid colored lines) and, for comparison, groups in several mass bins (dashed grey lines). In general we find a weak evolution of the quasar clustering with redshift. This can be simply explained by the evolution of the bias of its underlying host halo masses. In particular, the correlation length for luminous ($L > 10^9 L_\odot$) BHs tends to decrease slightly as a function of decreasing redshift until $z \sim 3$, following closely the bias of the $10^{11} - 10^{12} M_\odot$ groups (consistent with the constraints on the host masses of these BHs). At fixed mass, these groups are less biased as a function of decreasing redshift (Mo & White 2002; Bahcall et al.

2004). This is also in accord with our results from Figure 4, that the typical host halo mass remains roughly constant for $z > 3$. For lower redshift (particularly $z < 2$), we instead see a significant upturn in r_0 versus z , corresponding to the increase in typical host halo mass, just as we found in Figure 4 and Table 2. The lowest luminosity sources, however, show only minor change in r_0 , corresponding to a host mass which changes only slightly with redshift (consistent with the median host masses found in Table 2).

This luminosity dependence is sufficiently weak (less than a factor of 2 increase in r_0 across several orders of

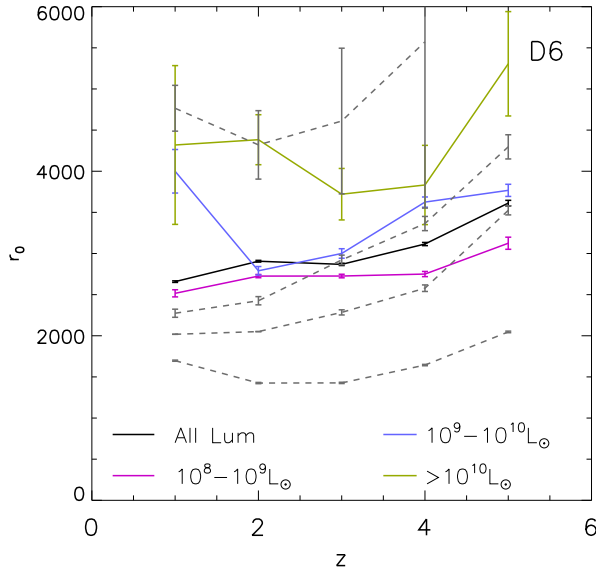


Figure 5. *Solid lines:* Black hole correlation length as a function of redshift for several luminosity bins (colored lines). *Grey dashed lines:* Group correlation length as a function of redshift for group mass ranges (from top to bottom) $> 10^{12} M_{\odot}$, $10^{11} - 10^{12} M_{\odot}$, $5 \times 10^{10} - 5 \times 10^{11} M_{\odot}$, $10^{10} - 10^{11} M_{\odot}$.

magnitude in luminosity) to remain broadly consistent with the predictions from models that suggesting bright and faint quasars occupy similar halos (e.g. Lidz et al. 2006; Bonoli et al. 2009). Indeed, our simulations produce complex lightcurves for our black holes, with luminosity varying rapidly across several orders of magnitude (see, e.g. Di Matteo et al. 2008; Degraf et al. 2010). This produces significant scatter in the relation between black hole luminosity and host mass, so general agreement with lightcurve-based models is expected (which are indeed motivated by simulations similar to our own). Nonetheless, as seen in Figure 2, there remains some correlation between BH instantaneous luminosity and group mass, so a weak dependence on luminosity is expected even in this model.

3.2 Small Scale Clustering

Although we find that the 2-halo terms for BHs and subgroups (galaxies) can be easily matched to provide a good estimator for typical host mass, there is significant discrepancy between their respective 1-halo terms (Figure 4, blue lines). The 1-halo BH correlation function is different both in shape and amplitude to the 1-halo term of galaxies, suggesting that, unlike at large scales, BHs do not cluster like their host galaxies on small scales. Or in other words, the distribution of BHs within halos does not follow closely that of their galaxies and hence does not trace the underlying matter distribution.

In terms of amplitude, $\xi_{\text{BH},1\text{h}}$ can be adjusted by only considering the BHs in those groups that match the mass range constrained by the 2-halo term, thereby minimizing the suppression of $\xi_{\text{BH},1\text{h}}$ from the numerous BHs in groups too small to contribute to the 1-halo term (due to hosting only a single BH). As expected, in this case, (Figure 4, green

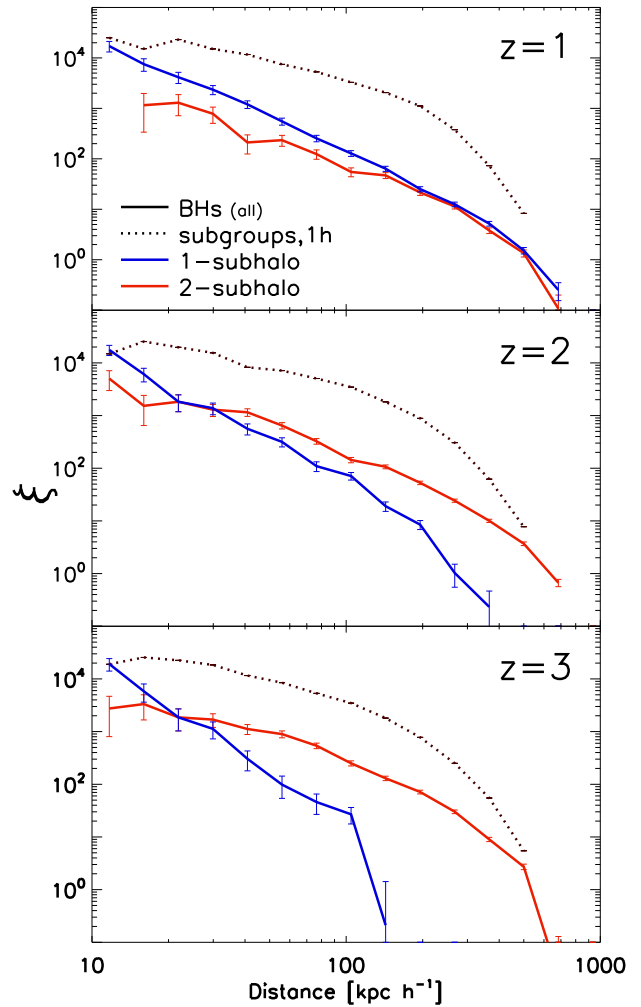


Figure 6. *Solid lines:* The 1-halo BH correlation function at $z=1,2,3$ divided into components from BH pairs occupying separate subhalos (red) or co-habiting a single subhalo (blue), using the full population of BHs. *Dotted lines:* The 1-halo subgroup correlation function at $z=1,2,3$.

line) the amplitude increases and is more in agreement with the 1-halo term of the subgroups ($\xi_{\text{subgroup},1\text{h}}$; at least at $z=1-3$ where the statistics are good enough).

It is, however, hard to account for the substantial difference in shape: $\xi_{\text{BH},1\text{h}}$ follows an approximate power law, lacking the decrease in slope at small scales (below $\sim 200 - 300 \text{ kpc h}^{-1}$) observed in $\xi_{\text{subgroup},1\text{h}}$ and expected from the 1-halo clustering produced by a general NFW profile (Navarro et al. 1996; Cooray & Sheth 2002; Zehavi et al. 2004). Thus the BHs are distributed significantly differently than an NFW profile, showing a significant boost at small scales.

We investigate the reason for this difference in the shape of the BH 1-halo term in terms of multiple BHs co-existing in a given subgroup. These BHs end up in a given subgroup as a result of mergers between their host galaxies, so that multiple BHs are expected to co-exist in a remnant (until dynamical friction is able to bring them close enough together to eventually merge).

To understand the effect this has on the small scale

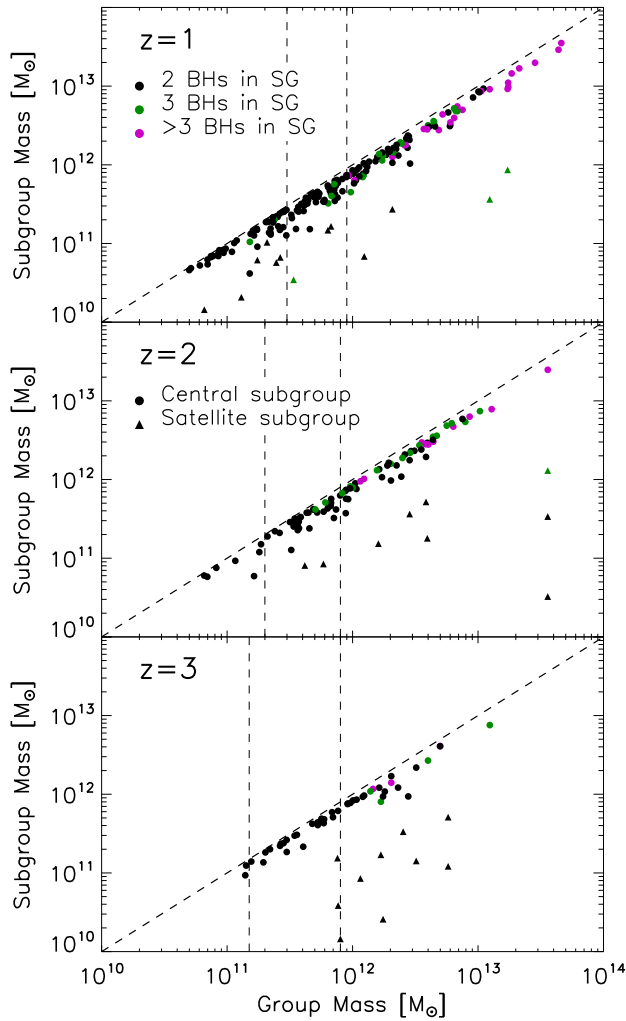


Figure 7. The mass of each subgroup containing at least 2 BHs vs. the mass of its host group. Color indicates number of BHs within the given subgroup: black - 2 black holes; green - 3 black holes; blue - 4 black holes; pink - more than 4 black holes. Symbol indicates if the subgroup is the primary (*i.e.* central) subgroup (circle), or a satellite subgroup (triangle). Dotted line: Represents a one-to-one mass ratio provided for reference.

clustering of BHs, we calculate the contributions to $\xi_{\text{BH},1\text{h}}$ from pairs of BHs occupying the same galaxy (we will call this the '1-subhalo' term) and from pairs of BHs occupying different galaxies within the same group ('2-subhalo' term), in analogy with dividing the overall correlation function into its 1-halo and 2-halo terms. We note that the existence of multiple BHs within a single subgroup necessarily indicates a previous merger event, since BH particles are not inserted into galaxies which already contain a BH particle, and thus any 1-subhalo contribution is inherently a result of previous galaxy mergers.

In Figure 6 we plot the 1-subhalo (solid blue) and 2-subhalo (solid red) components of $\xi_{\text{BH},1\text{h}}$, together with $\xi_{\text{subgroup},1\text{h}}$ for subgroups in groups within the mass ranges listed in Figure 4 (dotted line). The 1-subhalo term does indeed have a steeper slope than the 2-subhalo term, and is most significant at small scales. The 1-subhalo term is most dominant at low redshift, and by $z = 1$ it dominates the entire 1-halo term. This is a result of having increasingly large

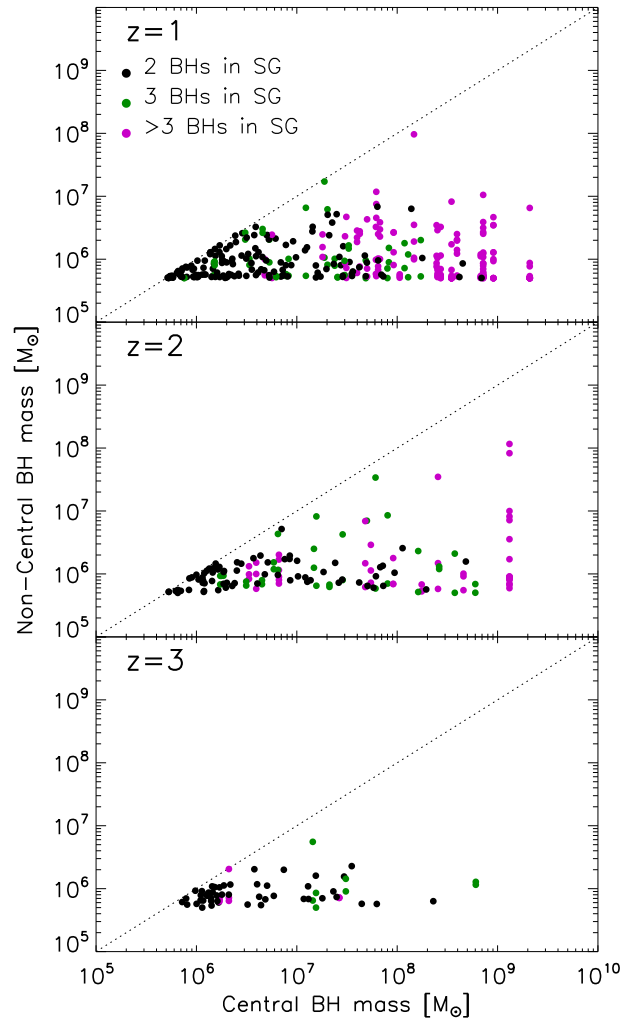


Figure 8. The mass of the central (largest) BH within a multiply-occupied subgroup relative to the mass of the non-central BHs within the same subgroup. Color indicates the number of BHs contained within the given subgroup: black - 2 black holes; green - 3 black holes; blue - 4 black holes; pink - more than 4 black holes. Dotted line: Represents a one-to-one mass ratio provided for reference.

groups at low redshift which have also undergone a relatively large number of mergers. These indeed contain multiply-occupied subgroups (see Figure 7). We also find that, if restricted to BHs within the same host mass range as the subgroups, the 2-subhalo term of $\xi_{\text{BH},1\text{h}}$ matches $\xi_{\text{subgroup},1\text{h}}$ quite closely. Thus we find that, within sufficiently large groups (such that the simulation contains enough groups hosting multiple BHs to produce a well-defined 1-halo term), $\xi_{\text{BH},1\text{h}}$ has two distinct components: one due to BH pairs which occupy separate galaxies, exhibiting good agreement with $\xi_{\text{subgroup},1\text{h}}$; and a steeper one caused by BH pairs which co-occupy individual galaxies as a result of previous galaxy mergers, causing a boost in the small-scale $\xi_{\text{BH},1\text{h}}$, particularly evident at low redshift, where typical groups are largest and have undergone significant merging.

In Figure 7 we plot the relative mass of each multiply-occupied subgroup and its host group, with circles indicating central subgroups, and triangles showing satellite subgroups. We clearly see that these multiply-occupied subgroups tend

to be the primary (central) subgroup within a given group, typically containing $\sim 65\text{--}70\%$ of the total group's mass. We also color-code the datapoints to show the number of BHs within each subgroup, and see that the central subgroup of larger groups tends to contain more BHs.

To investigate the masses of BHs which populate these multiply-occupied subgroups, in Figure 8 we plot the mass of the largest (primary) black hole within a given subgroup relative to the masses of the other BHs in the same subgroup, color-coded to show the number of black holes within the subgroup. In only a few rare cases do we have more than one massive BH, while in the majority of cases we have, at most, a single massive BH with one or more smaller black holes, generally within an order of magnitude of the seed mass. This suggests that the majority of BHs in multiply-occupied subgroups come from relatively small satellite subgroups (hosting correspondingly small black holes) which have fallen in and merged with the large, central subgroup, but do not grow substantially, instead remaining much less massive than the primary BH in the galaxy. Additionally, we observe that over time the fraction of BHs in the simulation located within these multiply-occupied subgroups increases from 2% at $z = 5$ to 15% at $z = 1$, as typical groups get larger and have had more opportunity for satellite subgroups to merge with the central subgroup. This increase in typical group mass causes an increase in both the number of multiply-occupied subgroups, as well as an increase in the typical number of black holes found within them (as seen in Figure 8), which produces the increased importance of the 1-subhalo term with decreasing redshift seen in Figure 6.

We will compare the small scale clustering from the simulations to observations in Section 3.4.

3.3 Quasar Bias

To further characterize the clustering properties of BHs, we now consider the quasar bias as a function of scale and redshift. The bias is obtained by taking the square root of the ratio between ξ_{BH} and the DM correlation function (shown as dotted lines in Figure 4). Based on our results of the small scale clustering, we expect the quasars to be strongly biased with respect to the DM distribution at small scales, particularly at high redshift. This general trend is clearly seen in Figure 4, where ξ_{DM} (dotted lines) increases with time (due to gravitational collapse), while ξ_{BH} tends to decrease slightly (seen more clearly in Figure 5). More importantly, we see that the BH clustering bias relative to that of DM is strongly scale-dependent, with ξ_{BH} exhibiting a significant increase in clustering at small scales (below $\sim 300 \text{ kpc h}^{-1}$) due to the strong 1-halo term, whereas ξ_{DM} shows only a slight increase at these small scales.

In the top of Figure 9 we plot the scale-dependent BH bias and subgroup bias (defined as $\sqrt{\xi_{\text{BH}}/\xi_{\text{DM}}}$; $\sqrt{\xi_{\text{subgroup}}/\xi_{\text{DM}}}$, respectively) found within the hosts of the best-fitting mass ranges found in Figure 4. Here we see that the subgroup bias levels off (as did ξ_{subgroup} in Figures 4 and 6), but the 1-subhalo term causes the BH bias to continue increasing to the smallest scales probed in our simulation. To show this more clearly, the middle of Figure 9 shows the bias of BHs relative to the subgroups ($\sqrt{\xi_{\text{BH}}/\xi_{\text{subgroup}}}$) for $z=1\text{--}5$. Within a given host

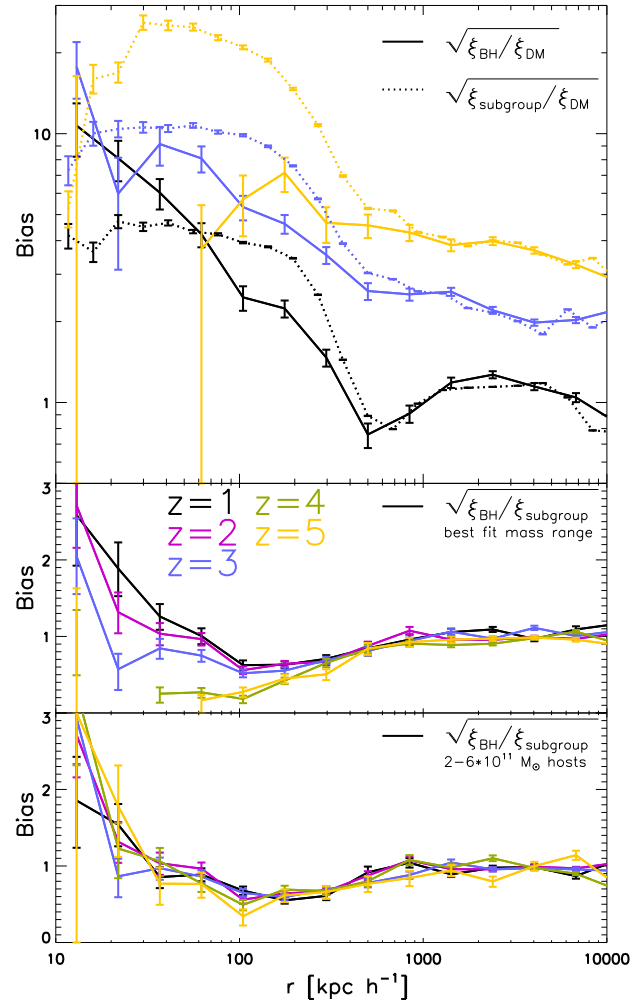


Figure 9. *Top:* Solid lines: Black hole bias defined as $\sqrt{\xi_{\text{BH}}/\xi_{\text{DM}}}$, using only BHs occupying halos in the best-fitting mass ranges specified in Figure 4. Dotted lines: Subgroup bias defined as $\sqrt{\xi_{\text{subgroup}}/\xi_{\text{DM}}}$, using only subgroups occupying halos in the best-fitting mass ranges specified in Figure 4. *Middle:* Bias of BHs relative to subgroups ($\sqrt{\xi_{\text{BH}}/\xi_{\text{subgroup}}}$) occupying halos in the typical mass ranges found in Figure 4. *Bottom:* Bias of BHs relative to subgroups ($\sqrt{\xi_{\text{BH}}/\xi_{\text{subgroup}}}$) occupying halos of mass $2 - 6 \times 10^{11} M_{\odot}$.

mass range, the BHs cluster very similarly to the subgroups (galaxies), except at the smallest scales (below $\sim 100 \text{ kpc h}^{-1}$), where we again see the increased clustering caused by the multiply-occupied subgroups remaining from merger events, as discussed earlier. Although we note that this small-scale bias appears to be redshift dependent, it is actually a result of the evolution of the host mass being considered. At higher redshifts, the typical host mass is smaller, and thus fewer will have undergone subgroup mergers producing multiply-occupied subgroups (as confirmed in Figure 7), thereby making the small-scale boost less apparent. When considering behavior for a fixed group mass (as shown in the bottom of Figure 9), we see that the bias between BH and subgroup clustering is redshift-independent, and consistently exhibits a strong small-scale boost from past subgroup mergers.

Table 2. Mean (median) halo mass of parent group and mean (median) luminosity of daughter BHs in D6 simulation.

	z=1	z=2	z=3	z=4	z=5
BH Luminosity					
All	39.9 (10.1)	24.2(9.07)	19.3 (9.51)	14.8 (8.34)	12.6 (8.34)
$10^8 L_\odot < L_{\text{BH}} < 10^9 L_\odot$	61.5 (18.7)	27.2 (9.66)	18.9 (8.80)	13.1 (7.53)	11.5 (7.12)
$10^9 L_\odot < L_{\text{BH}} < 10^{10} L_\odot$	252 (94.1)	54.9 (20.4)	38.2 (21.1)	25.5 (14.9)	15.9 (10.3)
Group Mass					
$M_{\text{group}} < 10^{11} M_\odot$	7.88 (7.69)	8.96 (8.55)	8.99 (8.83)	9.39 (9.25)	9.36 (9.34)
$10^{11} M_\odot < M_{\text{group}} < 10^{11.5} M_\odot$	8.66 (7.86)	9.09 (8.76)	9.39 (9.07)	9.54 (9.31)	9.71 (9.48)
$10^{11.5} M_\odot < M_{\text{group}} < 10^{12} M_\odot$	9.09 (8.23)	9.64 (9.19)	9.90 (9.42)	10.19 (9.64)	10.65 (9.88)
$10^{12} M_\odot < M_{\text{group}} < 10^{12.5} M_\odot$	9.45 (8.85)	10.19 (9.81)	11.16 (10.34)	10.82 (10.66)	10.92 (10.68)
$10^{12.5} M_\odot < M_{\text{group}}$	10.49 (9.51)	10.33 (10.20)	12.40 (11.49)	11.48 (11.54)	N/A
Log(Mean (Median) BH Luminosity) [$\log(L_\odot)$]					

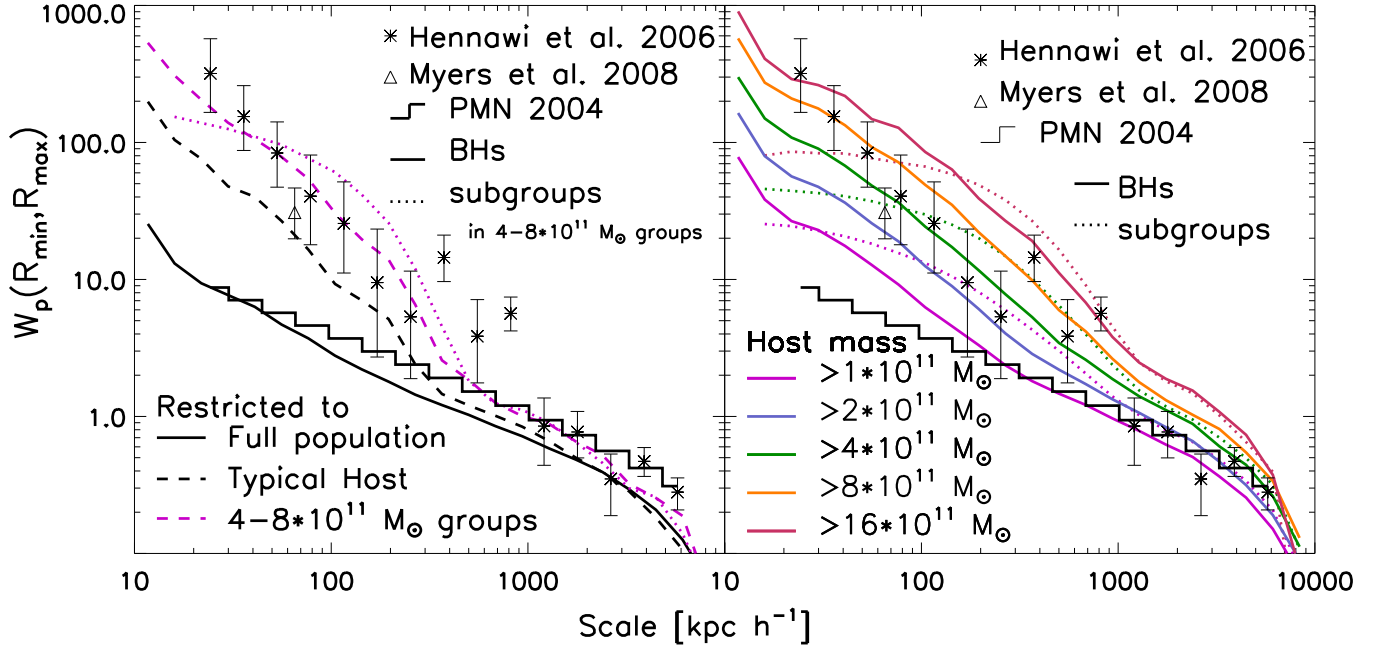


Figure 10. *Left:* The projected correlation function from the D6 simulation, averaged across redshifts 1-3, and across 3 projected directions for the full BH population (solid line), for BHs found within groups of the typical host mass shown in Figure 4 (dashed black line), for BHs found in groups of mass $4 - 8 \times 10^{11} M_\odot$ (dashed pink line), and for subgroups found in groups of mass $4 - 8 \times 10^{11} M_\odot$ (dotted pink line). We also plot the extension of the power law found in Porciani et al. (2004) (step function), and the observational results of Hennawi et al. (2006) (asterisks) and Myers et al. (2008) (triangle). *Right:* Same as left plot, but with $\bar{W}_P(R_{\min}, R_{\max})$ plotted for several lower-limits on the host group mass.

3.4 Comparison with observations: Projected Correlation Function

In order to compare with the observational constraints on the small scale clustering (see Hennawi et al. 2006; Myers et al. 2008), we compute the volume-averaged projected correlation function $\bar{W}_P(R_{\min}, R_{\max})$. This projected correlation function is computed using the same estimator described in Section 2.4, but the separation between points is the projected separation onto the xy , xz , or yz plane, rather than the separation in three-space. Although these three projections provide comparable results, we average across the three directions to avoid any potential directional bias. We then average across redshifts 1-3 (to match the

observational data redshift range), weighted by the number of BHs at each redshift, and plot the result in Figure 10, together with the data from Hennawi et al. (2006) (asterisks), Myers et al. (2008) (triangle), and the extension of the best-fit power law for the large scale clustering found by Porciani et al. (2004) (step-function). We have also plotted the projected correlation function for subhalos found in our simulations for several host mass ranges (dotted lines).

Figure 10 shows a remarkable agreement between the small scale clustering of BHs from the simulations with the observations. In particular, when considering BHs within groups in the mass range of $4 - 8 \times 10^{11} M_\odot$ the small scale boost (magenta line) matches the observed clustering very well. For completeness we also show (dashed black line) the

signal expected from BHs in the hosts of the typical mass ranges shown in Figure 4 which is also in good agreement, although slightly lower normalization. Indeed, the observed small-scale excess can be explained as resulting from the merger-based boost found in our simulations, further emphasizing the importance of such mergers on quasar evolution.

We also note that if the full BH population from our simulation is used, rather than those in the restricted mass range, we lose the small scale excess (solid line), since the majority of our BHs are found in groups too small to exhibit significant effects of subgroup mergers.

To investigate the dependence of the projected correlation function on the host mass in more detail, in the right of Figure 10 we plot $\overline{W}_P(R_{\min}, R_{\max})$ for BHs hosted by groups with several different lower-mass cutoffs (from 1 to $16 \times 10^{11} M_{\odot}$; colored lines), together with the observational data. Here we see that including less massive groups causes an overall decrease in amplitude (as expected), and also suppresses the small scale excess, as a result of smaller groups being less likely to host a multiply-occupied subgroup. This suggests that, given sufficient observational data, small-scale clustering may provide a sensitive means of probing the typical mass of merging pairs of galaxies hosting supermassive black holes. As shown, the curves with a lower mass cut of $\sim 4 - 8 \times 10^{11} M_{\odot}$ produce the best agreement with observation, implying that observed quasar pairs are typically located within groups of moderate size, comparable to those found within our simulation (and thus below the larger host masses typically associated with observed large-scale clustering).

4 CONCLUSIONS

In this paper we have investigated the clustering of black holes within hydrodynamic cosmological simulations, its redshift evolution, luminosity dependence, and particularly the small-scale behavior.

We have shown that the large scale clustering of black holes traces that of the galaxies within their host groups, and provides a predictor of the typical host mass, which for our simulations is found to be on the order of a few $10^{11} M_{\odot}$. Although well below the typically found masses of $\sim 2 \times 10^{12} - 10^{13} M_{\odot}$ (Lidz et al. 2006; Ross et al. 2009; Bonoli et al. 2009; Shen et al. 2009b), this is consistent with our limited simulation volumes which can only follow the growth of the faint-end of quasar population (DeGraf et al. 2010), and cannot follow formation of such massive groups. The typical host group mass shows some evolution with redshift, most significant below $z \sim 3$, where typical host masses increase by up to a factor 10 (at $z = 1$). This low-redshift increase is distinctly luminosity dependent, with the more luminous sources ($L_{\text{BH}} > 10^9 L_{\odot}$) undergoing the most substantial increase in typical host mass. Overall the evolution of clustering with redshift and luminosity is minor and consistent with current observational constraints (albeit in low luminosity populations this is yet to be fully constrained). The relatively weak dependence found in our simulations is consistent with the complex lightcurves we derive from our direct modeling in which quasar luminosities vary over relatively short timescales for a given host (as regulated by

hydrodynamical processes). This is also consistent with the models of Lidz et al. (2006).

In addition to the large-scale clustering (the 2-halo regime), our simulations allow us to study the small scale clustering (the 1-halo term) of ξ_{BH} . We found that $\xi_{\text{BH},1\text{h}}$ follows a power law behavior all the way to the smallest scales. The clustering of black holes at small scale is unlike that of galaxies (or dark matter). We showed that the 1-halo BH term can be subdivided into two components: 1-subhalo and 2-subhalo. The 1-subhalo term, $\xi_{\text{subgroup},1\text{h}}$, represents the clustering of BHs within a galaxy and 2-subhalo that of BHs occupying different galaxies. We have shown that the 1-subhalo is the one that provides the power law behavior, indicating that galaxies do contain multiple black holes as a result of mergers. These galaxies tend to be the central galaxy within relatively large groups (for our simulation), generally hosting at most a single massive BH with one or more smaller BHs, likely as a result of smaller satellite galaxies merging with the large, central galaxy within the group. In the absence of these multiply-occupied galaxies, $\xi_{\text{BH},1\text{h}}$ and $\xi_{\text{subgroup},1\text{h}}$ exhibit very close agreement, but the inclusion of these merger remnants causes a significant boost in the small-scale BH clustering. This merger-based boost is most significant at low redshift, where typical group size is largest, though we find it in sufficiently massive groups at all redshifts.

Though observational limitations make observing these scales difficult, several recent studies have found a small scale excess at scales below $\sim 100 \text{ kpc h}^{-1}$ (Hennawi et al. 2006; Myers et al. 2008). The observed excess is in remarkable agreement to the one predicted by our simulations coming from groups approaching $10^{12} M_{\odot}$, which host mostly intermediate size black holes. This suggests that multiple black holes co-occupying a subgroup at low redshifts are likely faint(ish) AGNs hosted in Milky Way size halos that have recently undergone merging. We also note that galaxies hosting multiple AGN (Komossa et al. 2003; Gerke et al. 2007; Barth et al. 2008; Comerford et al. 2009b) or inspiralling supermassive black holes (Comerford et al. 2009a) have been found in recent studies, further supporting our conclusion of multiply-occupied subgroups. Although we leave more detailed investigation of the small scale BH pairs in our simulations (particularly with regard to the luminosities of inspiralling black holes) for a future work, we note that our finding that multiply-occupied galaxies tend to host a single massive BH with one or more small BHs appears to be in keeping with the observation that most of the inspiralling BH pairs power only a single AGN (Comerford et al. 2009a). Given that, our agreement in small-scale merger-induced boost certainly reinforces the importance of galaxy mergers on the evolution of supermassive black holes. We also note this small-scale excess' sensitivity to the host mass suggests that future small-scale studies may provide a means to constrain the typical mass of merger events between galaxies hosting black holes, with current observational data combined with our simulations suggesting groups with typical masses comparable to those probed in our simulations (from a few $10^{11} M_{\odot}$ to $10^{12} M_{\odot}$) produce the multiply-occupied galaxies underlying the observed small scale excess.

We would like to point out however that there are several aspect of our modeling approach, including numerical

issues, in the simulations that potentially affect our results on the small-scale clustering. We have a very simplistic prescription to determine how BHs merge with one another (imposed by the limits on the resolution that can be achieved in these cosmological boxes). The current prescription has a BH pair merge when BHs are separated by less than their smoothing length and if the BHs relative velocity is small compared to the local sound speed. Changes to this prescription could accelerate (postpone) BH mergers, which would result in a suppression (increase) of our small scale clustering signals. It would be desirable to compare our results with other simulations which implement different prescriptions, or in the future to include more direct physical modeling of this region in higher resolution simulations. However, neither of these are currently possible. A numerical issue that may affect the results of our one-halo term is that black holes need to be fixed to potential minima (calculated among the neighboring particles within the smoothing length used for the accretion model) in order to avoid them leaving their subhalo due to numerical N-body noise (and the fact that dynamical friction is hard to calculate for sink particles). However, in some instances this may cause a BH particle in a small subhalo in orbit in a bigger group to 'hop' to the potential minimum of the larger group. This effect may be exacerbated in situations where the small subhalo may be stripped of gas by infalling into a larger one. These effects could artificially increase the number of BHs within large, central halos, thereby boosting small scale clustering. However, when we measure what fraction of BHs appear to 'hop' into the center of groups experiencing an unexpected jump in their position, we find that it is only $\sim 1 - 2\%$. Future simulations and comparison amongst different approaches (once they become available) should of course attempt to characterize these effects more specifically. We further note however, that observational studies have indeed found cases of galaxies hosting multiple BHs (Comerford et al. 2009a), so the existence of a one-subhalo term is expected. Additionally, as seen in Figure 10, the projected clustering of subgroups has a fundamentally different form than the observed quasar clustering. Thus the BHs cannot simply trace their host subgroups/galaxies and still produce the observed small scale excess, but rather a significant one-subhalo term is required to produce the small scale power law behavior.

In future work we also plan to simulate larger volumes (which we are starting to be feasible with the most advanced technology) to allow us to study clustering of AGN at larger (mass and length) scales while simultaneously investigating luminosity dependence for brighter sources more directly comparable to current and upcoming observational data, as well as providing increased statistics for the small scale clustering.

ACKNOWLEDGMENTS

This work was supported by the National Science Foundation, NSF Petapps, OCI-079212 and NSF AST-0607819. The simulations were carried out at the NSF Teragrid Pittsburgh Supercomputing Center (PSC).

REFERENCES

- Bahcall N. A., Hao L., Bode P., Dong F., 2004, *ApJ*, 603, 1
- Barth A. J., Bentz M. C., Greene J. E., Ho L. C., 2008, *ApJL*, 683, L119
- Bondi H., 1952, *MNRAS*, 112, 195
- Bondi H., Hoyle F., 1944, *MNRAS*, 104, 273
- Bonoli S., Marulli F., Springel V., White S. D. M., Branchini E., Moscardini L., 2009, *MNRAS*, 606
- Comerford J. M., Gerke B. F., Newman J. A., et al., 2009a, *ApJ*, 698, 956
- Comerford J. M., Griffith R. L., Gerke B. F., et al., 2009b, *ApJL*, 702, L82
- Cooray A., Sheth R., 2002, *Phys. Rep.*, 372, 1
- Croom S. M., Boyle B. J., Shanks T., et al., 2005, *MNRAS*, 356, 415
- Croom S. M., Shanks T., 1996, *MNRAS*, 281, 893
- Croton D. J., 2009, *MNRAS*, 394, 1109
- da Ângela J., Shanks T., Croom S. M., et al., 2008, *MNRAS*, 383, 565
- Degraf C., Di Matteo T., Springel V., 2010, *MNRAS*, 402, 1927
- Di Matteo T., Colberg J., Springel V., Hernquist L., Sijacki D., 2008, *ApJ*, 676, 33
- Di Matteo T., Springel V., Hernquist L., 2005, *Nature*, 433, 604
- Djorgovski S., 1991, in *The Space Distribution of Quasars*, edited by D. Crampton, vol. 21 of *Astronomical Society of the Pacific Conference Series*, 349–353
- Ferrarese L., Merritt D., 2000, *ApJL*, 539, L9
- Gebhardt K., Bender R., Bower G., et al., 2000, *ApJL*, 539, L13
- Gerke B. F., Newman J. A., Lotz J., et al., 2007, *ApJL*, 660, L23
- Graham A. W., Driver S. P., 2007, *ApJ*, 655, 77
- Haiman Z., Hui L., 2001, *ApJ*, 547, 27
- Hennawi J. F., Strauss M. A., Oguri M., et al., 2006, *AJ*, 131, 1
- Hewett P. C., Foltz C. B., Harding M. E., Lewis G. F., 1998, *AJ*, 115, 383
- Hopkins P. F., Hernquist L., Cox T. J., et al., 2005a, *ApJ*, 630, 705
- Hopkins P. F., Hernquist L., Cox T. J., Di Matteo T., Robertson B., Springel V., 2005b, *ApJ*, 630, 716
- Hopkins P. F., Hernquist L., Cox T. J., Di Matteo T., Robertson B., Springel V., 2005c, *ApJ*, 632, 81
- Hopkins P. F., Hernquist L., Cox T. J., Di Matteo T., Robertson B., Springel V., 2006, *ApJS*, 163, 1
- Hopkins P. F., Hernquist L., Martini P., et al., 2005d, *ApJL*, 625, L71
- Hoyle F., Lyttleton R. A., 1939, in *Proceedings of the Cambridge Philosophical Society*, vol. 35 of *Proceedings of the Cambridge Philosophical Society*, 405
- Kerscher M., Szapudi I., Szalay A. S., 2000, *ApJL*, 535, L13
- Kochanek C. S., Falco E. E., Muñoz J. A., 1999, *ApJ*, 510, 590
- Komossa S., Burwitz V., Hasinger G., Predehl P., Kaastra J. S., Ikebe Y., 2003, *ApJL*, 582, L15
- Kormendy J., Richstone D., 1995, *ARA&A*, 33, 581
- Kundic T., 1997, *ApJ*, 482, 631

- La Franca F., Andreani P., Cristiani S., 1998, *ApJ*, 497, 529
- Landy S. D., Szalay A. S., 1993, *ApJ*, 412, 64
- Lewis I. J., Cannon R. D., Taylor K., et al., 2002, *MNRAS*, 333, 279
- Lidz A., Hopkins P. F., Cox T. J., Hernquist L., Robertson B., 2006, *ApJ*, 641, 41
- Magliocchetti M., Porciani C., 2003, *MNRAS*, 346, 186
- Magorrian J., Tremaine S., Richstone D., et al., 1998, *AJ*, 115, 2285
- Martini P., Weinberg D. H., 2001, *ApJ*, 547, 12
- Mo H. J., Fang L. Z., 1993, *ApJ*, 410, 493
- Mo H. J., White S. D. M., 2002, *MNRAS*, 336, 112
- Mortlock D. J., Webster R. L., Francis P. J., 1999, *MNRAS*, 309, 836
- Myers A. D., Brunner R. J., Nichol R. C., Richards G. T., Schneider D. P., Bahcall N. A., 2007a, *ApJ*, 658, 85
- Myers A. D., Brunner R. J., Richards G. T., Nichol R. C., Schneider D. P., Bahcall N. A., 2007b, *ApJ*, 658, 99
- Myers A. D., Richards G. T., Brunner R. J., et al., 2008, *ApJ*, 678, 635
- Navarro J. F., Frenk C. S., White S. D. M., 1996, *ApJ*, 462, 563
- Padmanabhan N., White M., Norberg P., Porciani C., 2009, *MNRAS*, 397, 1862
- Peacock J. A., 1999, *Cosmological Physics*, *Cosmological Physics*, by John A. Peacock, pp. 704. ISBN 052141072X. Cambridge, UK: Cambridge University Press, January 1999.
- Porciani C., Magliocchetti M., Norberg P., 2004, *MNRAS*, 355, 1010
- Ross N. P., Shen Y., Strauss M. A., et al., 2009, *ApJ*, 697, 1634
- Shakura N. I., Sunyaev R. A., 1973, *A&A*, 24, 337
- Shen Y., Hennawi J. F., Shankar F., et al., 2009a, *ArXiv e-prints*
- Shen Y., Strauss M. A., Oguri M., et al., 2007, *AJ*, 133, 2222
- Shen Y., Strauss M. A., Ross N. P., et al., 2009b, *ApJ*, 697, 1656
- Springel V., White S. D. M., Tormen G., Kauffmann G., 2001, *MNRAS*, 328, 726
- Tremaine S., Gebhardt K., Bender R., et al., 2002, *ApJ*, 574, 740
- York D. G., Adelman J., Anderson Jr. J. E., et al., 2000, *AJ*, 120, 1579
- Zehavi I., Weinberg D. H., Zheng Z., et al., 2004, *ApJ*, 608, 16